

Magnetic-based Polydimethylsiloxane Microspheres for Magnetic Field Measurement

Bing Sun, Xinjiang Wang, Xiaobo Ma, Zhongyuan Sun, Zhiqiang Wang, Zuxing Zhang, and Kaiming Zhou

Abstract--Magnetic-based polydimethylsiloxane microspheres (MPMs) are fabricated and its applications for measurement of magnetic field are investigated. The MPMs are prepared by first incorporating the uniformly sized Mn₃O₄ nanocrystals into polydimethylsiloxane (PDMS) matrix, and then using a self-assembling method to obtain a chain of microspheres on the fiber taper. The MPMs are regarded as optical resonators, demonstrating whispering gallery modes (WGM) with a high Q factor in the 1310 nm band. Experimental results show that the resonance wavelengths of the WGM spectra depend on the strength of the magnetic field since the change in the applied field cause the mechanical deformation of the MPMs, leading to a shift in the resonant wavelength of the resonator. Using as magnetic field sensors, the performances of the MPMs in terms of sensitivities and measurement ranges have been optimized. Thus, the sensitivity of 101.9 pm/mT and the measurement range up to 8 mT are achieved with a MPM (~270 μm in diameter). Besides, the performance of the MPM after two-week storage is analyzed, showing the excellent long-term stability.

Index Terms--Optical fiber sensor, Magnetic sensor, whispering gallery modes, Magnetic nanoparticles, Polymer

I. INTRODUCTION

MAGNETIC field sensors that refer to a system for measuring magnetic flux, strength and/or direction of the magnetic field have been widely applied in applications including navigation, geophysical research, noncontact switching and biological activity mapping of human body organs [1]. Researchers have implemented a range of novel schemes for magnetic field measurement, including fluxgate sensor [2], Hall sensor [3], magnetoresistive sensors [4-5], MEMS sensor [6], and optical fiber magnetic field sensor (OFMFS) [7]. In terms of the sensing principle, most of OFMFSs need to rely on these magneto-optical properties, i.e., Faraday effect, magnetostrictive perturbation, tunable refractive index of magnetic fluids (MFs) [8]. Furthermore, the combination of various fiber schemes, such as microstructured

optical fibers [9-11], tapered fibers [12-13], microfiber couplers [14], functionalized gratings [15], or D-shaped fibers [16-17] have been reported towards the realization of high-sensitivity magnetic field measurement. For instance, an intensity sensitivity of 81 pm/mT based on an elliptical core fiber Bragg grating has been proposed by Gao et al. [18]. A temperature-compensated magnetic field sensor based on incorporating cascaded magnetostrictive alloy-fiber Bragg grating was achieved for the detection of magnetic field and temperature with sensitivities of 250 Hz/Oe and 1.97 or 1.42 kHz/ °C [19]. Recently, two magnetic field measurement methods by combining reflective Fabry-Perot interferometer with MF were present to obtain considerable sensitivities (268.81 pm/Gs from 15.5 to 139.7 Gs [20], 1.02602 nm/Gs from 118.768 to 166.261 Gs [21]).

Optical whispering-gallery-mode (WGM) resonator, which exhibits fine spatial and spectral confinement, could enable it an ideal platform for all kinds of sensors [22-23]. The WGM resonators have been intensively investigated in various geometries including disk [24], sphere [25], toroid [26] and bubble [27], which are usually made from inorganic materials (e.g., silica or semiconductors). Conventional silica-based WGM resonators are not competent for the measurement of magnetic field due to lack of sensitive elements. Thereupon, the MF-assisted hollow core fibers, photonic crystal fibers are used as micro-capillary based resonators, in which WGMs are intensively excited [28-32]. For instance, Mahmood et al. present a magnetic field sensitivity as high as 110 pm/mT, where the micro resonator was based on a length of photonic crystal fiber infiltrated with the MF containing nanoparticles with diameters of either 5 or 10 nm [28]. On the other hand, attempts were made to fabricate polymer-based WGM resonators with alternative materials (e.g., polydimethylsiloxane [33], poly (methyl methacrylate) [34], epoxy resin [35], SU-8 [36-37]). It implies that the polymer-based materials have the potential for fabricating multifunctional optical cavities not attainable by inorganic

This work was supported in part by National Natural Science Foundation of China under Grants 91950105 and 62175116, in part by Outstanding Chinese and Foreign Youth Exchange Program of China Association for Science and Technology (CAST), in part by the Jiangsu Province Science and Technology, the Association Youth Science and Technology Talent Promotion, in part by the 1311 Talents Program of Nanjing University of Posts and Telecommunications (Dingxin), in part by National Postdoctoral Program for Innovative Talents (BX201600077), in part by the Science Foundation of Nanjing University of Posts and Telecommunications (NY219046), and in part by China Postdoctoral Science Foundation (2017M611877), and in part by Marie Skłodowska-Curie Individual Fellowships in the European Union's

Horizon 2020 Research and Innovation Programme under Grant 891685. (Corresponding author: Zuxing Zhang and Zhiqiang Wang).

Bing Sun, Xinjiang Wang, Xiaobo Ma, Zuxing Zhang are with the Advanced Photonic Technology Lab, College of Electronics and Optical Engineering & College of Microelectronics, Nanjing University of Posts and Telecommunications, Nanjing 210023, China (e-mail: b.sun@njupt.edu.cn; wxj197207@163.com; maxiaobo@njupt.edu.cn; zxzhang@njupt.edu.cn).

Bing Sun, Zhiqiang, Kaiming Zhou are with the Aston Institute of Photonic Technologies, Aston University, Birmingham B4 7ET, UK (e-mail: z.wang35@aston.ac.uk; k.zhou@aston.ac.uk).

Zhongyuan Sun is with the School of Metallurgy and Materials, University of Birmingham, Birmingham B15 2TT, UK (e-mail: Z.Sun.2@bham.ac.uk)

materials. By taking advantage of the excellent flexibility of the polydimethylsiloxane (PDMS), Ioppolo et al. [38] first investigated the possibility of using magnetorheological PDMS spheres as micro-optical resonators, which show a very promising effect but a lower sensitivity of ~ 3 pm/mT. In addition, systematic investigations on how the size and concentration of the ferromagnetic particles, even the diameters of the microspheres play roles are lacking.

In this work, we have proposed a WGM-based resonator, which comprises of the magnetic-based polydimethylsiloxane microspheres (MPMs) for the high-sensitivity magnetic field measurement. Finer spatial confinement of the resonator leads to higher intensity and hence enhanced light matter interaction. Likewise, its excellent spectral confinement leads to longer photon lifetime which allows for repeated interaction of a photon with the matter, resulting again in the enhancement in light-matter interactions. The MPMs herein are prepared with two steps: The uniformly sized Mn_3O_4 nanocrystals are firstly achieved through the controllable synthesis process. Secondly, the Mn_3O_4 nanocrystals are incorporated in the PDMS through precursor doping method. Thereupon, a self-assembling method is employed to obtain a chain of microspheres on the fiber tapers. Note that the microspheres with various diameter and different nanoparticle volume can be characterized with high quality factors in the 1310 nm. Using as magnetic field sensors, the performances of the MPMs in terms of sensitivities and measurement ranges have been optimized. In special, the sensitivity of 101.9 pm/mT is obtained by the larger size of the MPMs while the magnetic field measurement ranges are increased with the smaller size of the MPMs.

II. PREPARATION OF MICROSPHERES

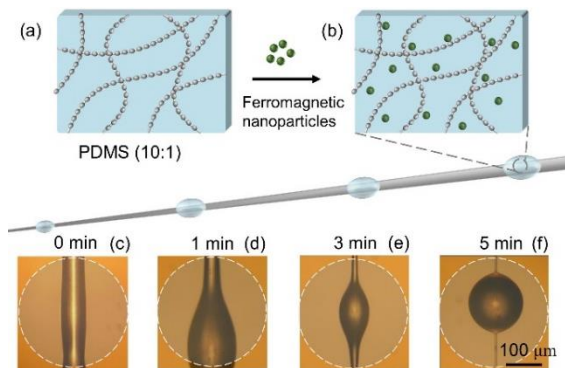


Fig. 1. Fabrication of the MPMs. (a) The primary cross-linking reaction of the PDMS occurs between the silicon hydride groups in the curing agent and vinyl groups in the monomer. (b) Mixture of Mn_3O_4 nanocrystals with PDMS. (c)-(f) Micrographs showing the self-assembled formation processes of MPMs over time (indicated in each image).

Manganese oxides, i.e., Mn_3O_4 nanocrystals are expected to find useful applications in catalysis, energy storage, magnetic data storage, ferrofluids, and sensors. Here the focus is to utilize the ferromagnetic properties of Mn_3O_4 nanocrystals for magnetic field sensing, and then the synthetic process for which is illustrated in the previously reported method (more details can be found in Appendix). Transmission electron microscopy (TEM) image of the synthesized Mn_3O_4 nanocrystals demonstrate that these nanocrystals are spherical in shape with

evenly dispersed distributions, as shown in Fig. A1. Note that the magnetic measurements were performed on a superconducting quantum interference device magnetometer (Quantum Design, MPMS XL7). The hysteresis loop for the synthesized Mn_3O_4 nanocrystals is shown in Fig. A2. After fully stirring the mixture of the Mn_3O_4 nanocrystals and the PDMS (RTV 184, Dow Corning 10:1, Fig. 1(a)), the precursor is subjected to an ultrasonic bath for 30 min to attain uniformly dispersed nanocrystals. The bath sonication is performed in an ice-water mixture to prevent the rapid polymerization of PDMS by ultrasound heating. Afterwards the embedded nanocrystals in PDMS matrix are successfully prepared, as shown in Fig. 1(b). It is worthy noting that the situation of the dispersed nanocrystals in PDMS (e.g., the precursor clearance, the nanocrystals cluster, etc.) is conceptually similar to those regular distribution involved in the TEM image (the inset in Fig. S1) since the TEM specimens are made by evaporating drops of reaction solution onto carbon-coated copper grids, which can be found in Ref. [39]. On the other hand, the optical characterizations in section IV, i.e., the Q factors of the microspheres are highly related to the concentration are indirectly verified for the impossibility of the Mn_3O_4 nanocrystals cluster.

Initially, the tapered fibers were fabricated and made the hydrophobic treatment. And a drop of the doped PDMS was placed on the surface of the tapered fiber by utilizing tungsten or fiber probes. It results in a fractal pattern of main droplets around the drop location of the tapered fiber (Fig. 1(c)), and the typical droplets of different diameters over time are shown in Figs. 1 (d-f). Due to its surface tension, the droplets ‘want’ to move to the thinner region (Fig. 1(f)). There are, in fact, satellite and subsatellite microsphere formations be observed down to the 3rd and 4th generations around the thinner region (Fig. S3) as the transformation process is recorded by taking micrographs in real time. As a result, a uniform magnetic PM with various diameters could be manipulated with desired pattern and formed after thermal treatment. It’s worth noting that the tapered fibers with different geometric parameters and the viscosity of the doped PDMS would significantly contribute to produce a chain of MPMs with various diameters.

III. PRINCIPLE

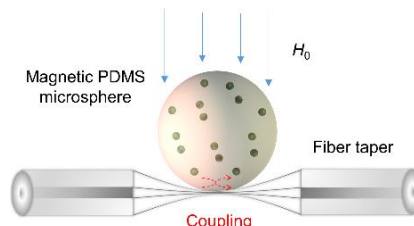


Fig. 2 Schematic of the MPM in the presence of a static, uniform magnetic field of H_0 .

In principle, the polymer microsphere can be regarded as an optical resonator. The laser light from the fiber taper is nearly tangentially coupled into the microsphere and then approaching to the interior surface of the sphere beyond the critical angle, thereby experiencing a total internal reflection along the interior surface of the microsphere. When trapped inside the polymer

microsphere in diameter of several hundred microns, light could circulate in a WGM over millions of times. Thus, the resonances are realized when light returns to its starting location in phase. And the approximate condition for resonances are

$$2\pi n_0 a = m\lambda \quad (1)$$

where λ is the wavelength of the laser, n_0 and a are the refractive index and the radius of microsphere, respectively, and m is an integer indicating the circumferential mode number. Note that Eq. (1) is a first order approximation and holds for $a \gg \lambda$. At resonances, light experiences constructive interference in the microsphere, which can be observed as dips in the transmission spectrum through the optical fiber taper. Here we consider the MPMs (with different volume fraction of nanoparticles, ϕ) under a static, uniform magnetic field of H_0 as depicted in Fig. 2. The external magnetic field instigates a stretching or compacting force within the microsphere. The change in the resonance wavelength due to the refractive index (dn/n) is negligible compared to the size effect (da/a). According to the Ref. [38], the shift can be obtained by solving the Navier equation to obtain the deformation of the sphere:

$$\frac{d\lambda}{\lambda} = \frac{da}{a} = \frac{7-4\nu}{4G(7+5\nu)} \frac{3B_0^2(\mu_r - 1)^2}{\mu_0(\mu_r + 2)^2} \quad (2)$$

where ν is the Poisson ratio, G is the shear modulus, $B_0 = \mu_0 H_0$, and μ_r is magnetic permeability. Thus, a minute change in the size of the microsphere will lead to the resonance shift of the WGM.

IV. EXPERIMENTAL RESULTS

A simply-equipped optical coupling system including 3-D translation stages and a microscopic manipulation setup is used to evanescently couple the microsphere to a micro/nano optical fiber (MNOF, taper waist: $\sim 1 \mu\text{m}$). The MPM supported by the tapered fiber is firstly placed on the glass slide, which are thus mounted on a 1-D stage (only adjustment device of the height is required). Considering that the optical coupling efficiency is dependent on the amounts of field overlap and phase matching, the spatial location between the MNOF and the MPM can be achieved by using the mentioned optical coupling system. When the phase matching is achieved, light is trapped within the microresonator by almost total internal reflections from the microsphere's curved surface. After running a circle, the wave returns to the same point with the same phase, the WGMs thus arise.

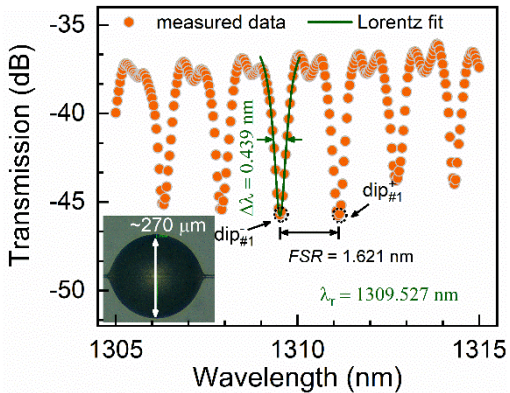


Fig. 3 Transmission spectrum of a MPM ($\sim 270 \mu\text{m}$ in diameter). Inset: optical micrograph of the MPM.

Initially, the microsphere with $\sim 270 \mu\text{m}$ in diameter (e.g., sample #1 with $\phi = 20\%$) is fabricated, where its spectrum is depicted in Fig. 3. The quality of the spectrum can be characterized by the factor as $Q = \lambda_r/\Delta\lambda$, where λ_r is the resonance wavelength and $\Delta\lambda$ represents the full width at half maximum (FWHM) value of the resonant wavelength and can be calculated from the transmission spectrum [40]. Fine transmission spectrum around 1310-nm band is fit well with Lorentzian-shaped line and the Q is calculated to be 2.983×10^3 . Moreover, the experimentally evaluated free spectrum range (FSR), in terms of wavelength (λ_r), is comparable with the theoretically estimated value based on the formula of $\lambda_r^2/(n\pi a)$. For instance, the experimentally observed FSR is 1.621 nm and the corresponding theoretically calculated value is 1.42 nm.

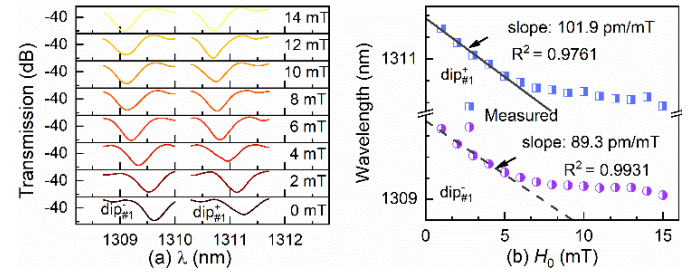


Fig. 4 (a) Fine WGM spectra (sample #1) correspond to the strength. (b) The wavelength shifts of $\text{dip}_{\#1}^+$, $\text{dip}_{\#1}^-$ as function of the field strength.

We study the dependences of the sample #1 in terms of the fine WGM spectra around 1310-nm band in presence of the small magnetic field strength. As shown in Fig. 4(a), the magnitudes of the resonant peaks (e.g., $\text{dip}_{\#1}^-$, $\text{dip}_{\#1}^+$) present no obvious change while the shifts move toward shorter wavelengths. Furthermore, the linear responses which are shown in Fig. 4(b) are concluded with sensitivities up to 101.9 pm/mT and 89.3 pm/mT for $\text{dip}_{\#1}^-$ and $\text{dip}_{\#1}^+$, respectively, which confirms our speculation. And the results are comparable with the Ref. [28] but with better R^2 values of 0.9931 and 0.9761, respectively. In addition, the magnetic field detecting range of the sample #1 reaches approximately to be 8 mT.

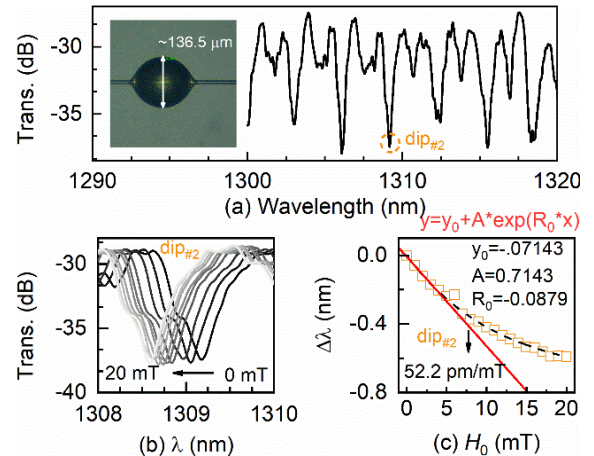


Fig. 5 (a) Transmission spectrum of a $\sim 136.5 \mu\text{m}$ -diameter MPM. (b) The transmission resonance, i.e., dip#2 corresponds to the strength. (c) The shift of dip#2 as function of the strength.

Thus, we utilize a smaller size of the MPM ($\sim 136.5 \mu\text{m}$ in diameter, sample #2) with the same concentration of $\phi = 20\%$.

Figure 5(a) shows the WGM spectrum of the sample #2 while the reduced size of the optical resonator evidently leads to the enlarged FSR, which agrees well with theoretical formula. As shown in Fig. 5(b), the WGM resonances experience ‘blue’ shift and show no amplitude variation as the magnetic field increases. Such wavelength shift behaviors can be attributed to the fact that Mn_3O_4 nanocrystals exert force upon each other because of dipolar interactions in presence of the magnetic field, thus, these forces lead to changes in the mechanical. Thereupon, the shift of the WGM resonances, exemplified by dip_{#2}, which are shown in Fig. 5(c), can be fit well by the exponential function, predicting the magnetic responses also occur in the microsphere with such small diameter, with a saturated magnetic field up to a value larger than 16 mT. We can speculate that the saturation is caused by the complete alignment of all ferromagnetic nanoparticles with the applied field, consequently leading to no further changes in the size. Nevertheless, the linear response of the sensing element would allow accurate detection of minute magnetic field variations across the detection range. The linear response of the sample #2 shows a sensitivity of 52.2 pm/mT. It’s acknowledged that the accumulated amounts of nanoparticles in the larger microsphere are decreased, which consequently can make less contribution to the sensitivity. It is due to that the sensitivity of the larger MPM (sample #1) is more than that of the smaller one (sample #2), greater magnetic field strength tolerance is essential to ensure that both MPMs have equivalent exerting force. It’s concluded that the sensitivity is significantly dependent on the size of the MPM.

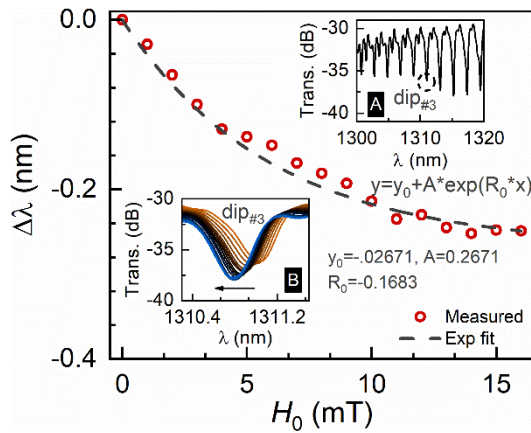


Fig. 6 Resonance shift (e.g., dip_{#3}) of sample #3 as a function of the field strength. Inset A: the initial transmission spectrum. Inset B: enlarged view of transmission spectra when the magnetic field is applied.

The aforementioned behaviors can be displayed in another MPM with lower concentration of nanocrystals while its diameter is $\sim 200 \mu\text{m}$. Figure 6 depicts the magnetic dependence of the MPM with $\phi = 10\%$ while the transmission spectrum and the details around $\lambda = 1310 \text{ nm}$ are shown in the insets. Note that the shear modulus of the MPM can be described with good approximation by $G = G_0 (1 + 2.5\phi + 14.1\phi^2)$, where G_0 is the shear modulus of the pure polymer [38]. And the shear modulus is modified when subjected to a magnetic field. As expected, the corresponding linear sensitivity is smaller than that of other samples (sample #1, sample #2) due to the lower concentration

of Mn_3O_4 nanocrystals. Regardless of its low sensitivity, the measurement range can be broadened up to 12 mT, which further confirm our speculation. We seek to understand nature of the behavior behind the saturation of the MPM in the presence of magnetic field in follow-up work.

V. DISCUSSION

Spectral confinement and losses are typically discussed using the quality factor (Q) or linewidth of the resonance mode ($\Delta\lambda$). Linewidth in sensing applications is crucial because it puts a limit on the resolvability of frequency shift. For instance, a large linewidth (i.e., bad spectral confinement, large loss) will not allow resolving small frequency shifts. As shown in Fig. 7, the Q values of the MPMs in terms of three different concentrations of the Mn_3O_4 nanocrystals are calculated in accordance with the formular ($Q = \lambda_r/\Delta\lambda$). As a result of which the FWHM ($\Delta\lambda$) is gradually broadened, the Q value slightly goes down when the concentration is increased. Besides, the transmission spectra would be more complicated with the larger concentration of nanocrystals (e.g., R^2 of the Lorentzian fit is decreased) though the relative sensitivity is increased. For instance, the spectral response of the samples shows a series of valleys between mainly consecutive resonances though a little more attention is necessary to find the similar explanation [41], which is considered due to the excitation of higher-order radial modes by the low effective index fiber taper and the non-degenerate higher-order angular modes associated with the microsphere ellipticity. It’s believed that the MPM with higher concentration might induce inter-modal coupling [42–43]. The tradeoff between the sensitivity, the quality factor and the modal coupling would be significantly considered in future work.

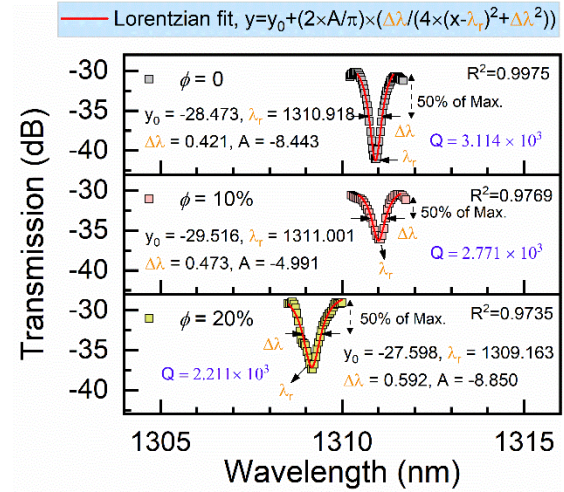


Fig. 7 The transmission spectra of the high-quality modes versus different concentrations of nanocrystals together with a Lorentzian fit.

The performances of different WGM-based static magnetic field sensors are compared in Table 1. The sensitivity of the proposed sensor is higher than that of the magnetic field sensor using the magnetic-fluid-filled silica microcapillary optofluidic ring resonator (OFRR) [29]. Likewise, Zhang et al. took advantage of a corrosive hollow-core fiber to improve the sensitivity [31]. By means of using similar structure, a

sensitivity of 0.4 dB/mT was present [32]. Although Mahmood et al. [28, 30] replaced microcapillaries with photonic crystal fibers (PCFs) and obtained the considerable sensitivities, the Q-factors achieved for the microresonators were 4.24×10^3 and 1.975×10^3 , which could be improved with alternative cavities. It's acknowledged the hollow resonators can be roughly divided into two categories: bottle-like resonators and the microbubble resonators and have merits such as high sensitivity and convenient integration with microfluidics. However, most WGM-based magnetic field sensors are employed with the magnetic fluid, which draws into the evaporation and structural instability, thus, greatly limits their practical applications. By contrast, the solid resonators can have good points of simple structure, low production cost, strong mechanical stability, and good robustness [44]. Ioppolo et al. utilized a magnetorheological PDMS sphere to achieve magnetic field measurement despite the low sensitivity [38].

TABLE I Performances of Optical Fiber Magnetic Field Sensors Based on the WGM

Fiber scheme	Sensing element	Q-factor	Sensitivity (pm/mT)	Ref.
OFRR	MF	2.58×10^3	75.7	[29]
Corrosive HCF	MF	3.4×10^3	324	[31]
Thin-wall HCF	MF	2.698×10^4	* 0.4 dB/mT	[32]
PCF	MF	4.24×10^3	110	[28]
PCF	ferronematic materials	1.975×10^3	[†] -61.86, -49.88	[30]
Microsphere	Magnetorheological PDMS	2×10^6	~ 3	[38]
Microsphere	Magnetic-based PDMS	6.264×10^3	101.9	This article

*Intensity sensitivity; [†]-61.86 for rod like, -49.88 for spherical like ferromagnetic suspensions

In order to demonstrate the long-term stability of the MPM, we compare the performances of the sample #3 before and after two weeks. As shown in Fig. 7(a), the transmission spectra of sample #3 obtained after two-week storage show similar profile to the initial spectrum. The evaluated FSRs present no change, which is 2.08 nm and 2.09 nm , respectively. Fig. 7(b) shows the resonant wavelength shift of the sample #3 in 1310-nm band as a function of the external magnetic field. It can be easily observed that the resonance shifts after two-week storage shows a slight change at the beginning of the applied field strength, then it presents negligible difference when the magnetic field is further increased. A longer-term trial (e.g., one year) is in essential and would be carried out in order to characterize the excellent stability of the polymer-based resonators.

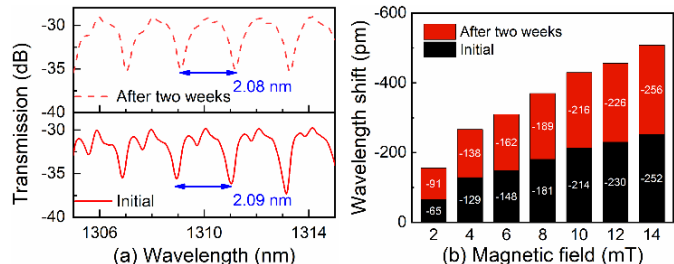


Fig. 8 Characterization of the MPM for magnetic sensing. (a) Typical transmission spectra before and after two weeks. (b) Resonance shift versus the magnetic field in a range of 0-14 mT.

Our results provide clear evidence for the flexibility of the magnetic based PDMS by directly incorporating ferromagnetic particles, i.e., Mn_3O_4 nanocrystals in the polymer matrix, and the MPMs with various diameter fabricating by means of the self-assembling method as described above. We demonstrate the MPM as an optical resonator can be utilized for high-sensitivity magnetic sensing. The performances of the MPMs could be optimized by various diameters of microspheres and different particle volumes. In comparison to the previous reported work [38], the proposed MPMs take advantage of ferromagnetic nanoparticles to obtain a high magnetic sensitivity. The fine size control in the microspheres is yet a challenge while it probably be improved after optimization of the attached surface of the tapered fiber and the viscoelasticity of PDMS. Moreover, the robustness of such microsphere-taper systems can be improved using the UV curable epoxy [45] or PDMS [37] packaging technique. Note that polymer encapsulation process should be carefully implemented in order to not reduce the performance of the WGM-based system. As a result, the package is demonstrated to work outside the optical bench and could be applied in the application test. Thus, the sensors with the package can be implemented to measure the dynamic magnetic fields [44].

VI. CONCLUSION

In summary, we have fabricated the high-Q MPMs using a simple and highly efficient method and investigated the magnetic response of the WGMs in detail. The high magnetic sensitivity, excellent flexibility, and long-term stability make the MPM a promising candidate for small magnetic sensing. The flexible platform can be developed into state-of-the-art of ultrasensitive sensors and microlasers as other functionalized materials could be dissolved into the polymer solutions, to give it a wide range of applications. Besides, the proposed optical resonator can be miniaturized into a compact and portable device.

VII. ACKNOWLEDGMENT

The authors would like to appreciate the reviewers for the valuable comments that improved the manuscript.

VIII. APPENDIX

The paragraphs regard to the preparation of Mn_3O_4 nanocrystals and magnetic-based polydimethylsiloxane matrix.

1. Materials and methods

1.1. Materials

All chemicals used in this experiment were commercially available without further purification. Sylgard 184 Silicon Elastomer and curing agent were obtained from Sigma Aldrich.

1.2. Preparation of Mn_3O_4 nanocrystals

a. Manganese stearate ($\text{Mn}(\text{SA})_2$): A MnCl_2 solution dropped into an aqueous solution of sodium stearate at 95°C , then the $\text{Mn}(\text{SA})_2$ was obtained. After washing with hot water and dried it at 60°C in vacuum oven, the powder $\text{Mn}(\text{SA})_2$ was obtained.

b. Mn_3O_4 nanocrystals were prepared as follows: $\text{Mn}(\text{SA})_2$

0.1866g, dodecylamine 1.5 g and 15 mL toluene was added to a beaker and heated to 90 °C until it becomes a dark brown transparent solution. The solution was then cooled to natural temperature. Next, 0.6 mL tertbutylamine and 45 mL water were loaded into the autoclave. The above mixture solution was slowly poured into the autoclave. Then put the autoclave into the oven and heated it to 180 °C for 5h without stirring. The crude solution of Mn_3O_4 nanocrystals was deposited to separate by magnetic and remove impurities.

Fig. S1 shows that these Mn_3O_4 nanocrystals are spherical in shape with evenly dispersed distributions. By counting over 100 Mn_3O_4 nanocrystals for many samples from transmission electron microscopy (TEM) image (the inset), the average size of these Mn_3O_4 nanocrystals is 9.2 nm. Furthermore, the synthesized Mn_3O_4 nanocrystals are analyzed by using a vibrating sample magnetometer at the temperature of 5 K. The hysteresis loop for the sample is shown in Fig. S2, and the saturation magnetization for the Mn_3O_4 nanocrystals is 14.42 emu/g.

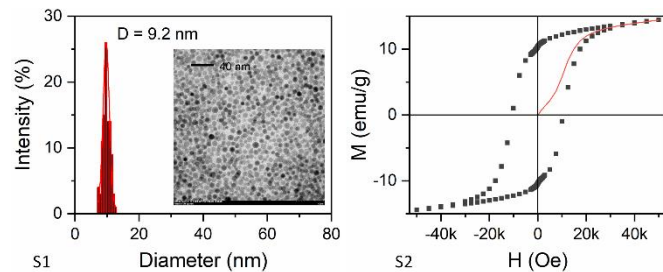


Fig. S1 Size distribution histogram of various sized Mn_3O_4 nanocrystals with the TEM image in the inset. S2 Hysteresis loop with maximum applied field equal to 55 kOe at the temperature of 5 K.

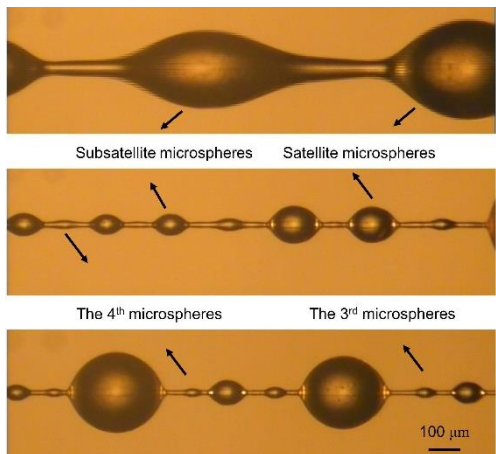


Fig. S3 Optical images of the transformation process. Various microspheres with different diameters can be obtained after thermal treatment. Satellite and sub-satellite, the 3rd and 4th generations are labelled in the images.

IX. REFERENCES

- [1] J. Lenz and S. Edelstein, "Magnetic sensors and their applications," *IEEE Sensors Journal* 6(3): 631-649 (2006)
- [2] F Primdahl, "The fluxgate magnetometer," *J. Phys. E: Sci. Instrum.* 12 241 (1979)
- [3] P.-A. Besse, G. Boero, M. Demierre, V. Pott, and R. Popovic, "Detection of a single magnetic microbead using a miniaturized silicon Hall sensor," *Appl. Phys. Lett.* 80, 4199 (2002)
- [4] M. Pannetier, C. Fermon, G. Le Goff, J. Simola, and E. Kerr, "Femtotesla Magnetic Field Measurement with Magnetoresistive Sensors," *Science* 304, 1648 (2004)
- [5] N. A. Stutzke, S. E. Russek, and D. P. Pappas, "Low-frequency noise measurements on commercial magnetoresistive magnetic field sensors," *Journal of Applied Physics* 97, 10Q107 (2005)
- [6] M., Stephan, J. Robert, G. Henry, Q. Eckhard, K. Reinhard, W. Bernhard, "MEMS magnetic field sensor based on magnetoelectric composites," *J. Micromech. Microeng.* 22, 065024 (2012)
- [7] É. Pinet, "Saving lives," *Nature Photon* 2, 150–152 (2008)
- [8] C. Liu, T. Shen, H. Wu, Y. Feng, J. Chen, "Applications of magnetostrictive, magneto-optical, magnetic fluid materials in optical fiber current sensors and optical fiber magnetic field sensors: A review," *Optical Fiber Technology* 65, 102634 (2021)
- [9] H. Thakur, S. Nalawade, S. Gupta, R. Kitture, and S. N. Kale, "Photonic crystal fiber injected with Fe₃O₄ nanofluid for magnetic field detection", *Applied Physics Letters* 99: 161101 (2011)
- [10] R. Gao, Y. Jiang, and Yang Zhao, "Magnetic field sensor based on anti-resonant reflecting guidance in the magnetic gel-coated hollow core fiber," *Optics Letters* 39: 6293-6296 (2014)
- [11] M. Deng, C. Huang, D. Liu, W. Jin, and T. Zhu, "All fiber magnetic field sensor with Ferrofluid-filled tapered microstructured optical fiber interferometer," *Opt. Express* 23: 20668-20674 (2015)
- [12] A. Layeghi, H. Latifi, and O. Frazão, "Magnetic Field Sensor Based on Nonadiabatic Tapered Optical Fiber with Magnetic Fluid," *IEEE Photonics Technology Letters*, 26(19): 1904-1907 (2014)
- [13] B. Sun, F. Fang, Z. Zhang, J. Xu, and L. Zhang, "High-sensitivity and low-temperature magnetic field sensor based on tapered two-mode fiber interference," *Optics Letters* 43: 1311-1314 (2018)
- [14] L. Mao, S. Pu, D. Su, Z. Wang, X. Zeng, and M. Lahoubi, "Magnetic field sensor based on cascaded microfiber coupler with magnetic fluid," *Journal of Applied Physics* 120, 093102 (2016)
- [15] Y. Miao, K. Zhang, B. Liu, W. Lin, H. Zhang, Y. Lu, J. Yao, "Ferrofluid-Infiltrated Microstructured Optical Fiber Long-Period Grating," *IEEE Photonics Technology Letters*, 25(3): 306-309 (2013)
- [16] G. Violakis, N. Korakas, and S. Pissadakis, "Differential loss magnetic field sensor using a ferrofluid encapsulated D-shaped optical fiber," *Optics Letters* 43: 142-145 (2018)
- [17] Z. Jiang, J. Dong, S. Hu, Y. Zhang, Y. Chen, Y. Luo, W. Zhu, W. Qiu, H. Lu, H. Guan, Y. Zhong, J. Yu, J. Zhang, and Z. Chen, "High-sensitivity vector magnetic field sensor based on side-polished fiber plasmon and ferrofluid," *Optics Letters* 43: 4743-4746 (2018)
- [18] R. Gao, D. Lu, Q. Zhang, X. Xin, Q. Tian, F. Tian, and Y. Wang, "Temperature compensated three-dimension fiber optic vector magnetic field sensor based on an elliptical core micro fiber Bragg grating," *Opt. Express* 28, 7721-7733 (2020)
- [19] D. Feng, Y. Gao, T. Zhu, M. Deng, X. Zhang, and L. Kai, "High-Precision Temperature-Compensated Magnetic Field Sensor Based on Optoelectronic Oscillator," *J. Lightwave Technol.* 39, 2559-2564 (2021)
- [20] Y. Zhao, X. Wang, R. Lv, H. Zheng, Y. Zhou and M. Chen, "Reflective Highly Sensitive Fabry-Perot Magnetic Field Sensor Based on Magneto-Volume Effect of Magnetic Fluid," *IEEE Transactions on Instrumentation and Measurement* 70, 1-6 (2021)
- [21] Y. Zhao, X. Wang, R. Lv, G. Li, H. Zheng and Y. Zhou, "Highly Sensitive Reflective Fabry-Perot Magnetic Field Sensor Using Magnetic Fluid Based on Vernier Effect," *IEEE Transactions on Instrumentation and Measurement* 70 1-8 (2021)
- [22] F. Vollmer, S. Arnold, "Whispering-gallery-mode biosensing: label-free detection down to single molecules," *Nat Methods* 5, 591–596 (2008)
- [23] X. Xu, W. Chen, G. Zhao, Y. Li, C. Lu and L. Yang, "Wireless whispering-gallery-mode sensor for thermal sensing and aerial mapping," *Light Sci Appl* 7 62 (2018)
- [24] R. Boyd and J. Heebner, "Sensitive disk resonator photonic biosensor," *Appl. Opt.* 40, 5742-5747 (2001)
- [25] Y. Zhang, T. Zhou, B. Han, A. Zhang, and Y. Zhao, "Optical bio-chemical sensors based on whispering gallery mode resonators," *Nanoscale* 10, 13832–13856 (2018)
- [26] S. M. Spillane, T. J. Kippenberg, K. J. Vahala, K. W. Goh, E. Wilcut, and H. J. Kimble, "Ultrahigh-Q toroidal microresonators for cavity quantum electrodynamics," *Phys. Rev. A* 71, 013817 (2005)
- [27] M. Sumetsky, Y. Dulashko, and R. Windeler, "Super free spectral range tunable optical microbubble resonator," *Opt. Lett.* 35, 1866-1868 (2010)
- [28] A. Mahmood, V. Kavungal, S. Ahmed, G. Farrell, and Y. Semenova, "Magnetic-field sensor based on whispering-gallery modes in a photonic

- crystal fiber infiltrated with magnetic fluid," *Optics Letters* 40: 4983-4986 (2015)
- [29] S. Zhu, L. Shi, N. Liu, X. Xu and X. Zhang, "Magnetic field sensing using magnetic-fluid-filled optofluidic ring resonator," *Microfluid Nanofluid* 21, 156 (2017)
- [30] A. Mahmood, V. Kavungal, S. Ahmed, P. Kopcansky, V. Zavisova, G. Farrell, and Y. Semenova, "Magnetic field sensing using whispering-gallery modes in a cylindrical microresonator infiltrated with ferroelectric liquid crystal," *Opt. Express* 25, 12195-12202 (2017)
- [31] Y. Zhang, N. Zhu, P. Gao, Y. Zhao, "Magnetic field sensor based on ring WGM resonator infiltrated with magnetic fluid," *Journal of Magnetism and Magnetic Materials* 493, 165701 (2020)
- [32] J. Zhang, C. Tian, R. Wang, H. Chen, X. Zhang, Z. Guo, W. Wang, "Fiber-optic whispering-gallery-mode magnetic field sensor based on magnetic fluid infiltrated hollow core fiber," *Microw Opt Technol Lett.* 63, 2442-2448 (2021)
- [33] C. Dong, L. He, Y. Xiao, V. Gaddam, S. Ozdemir, Z. Han, G. Guo and L. Yang, "Fabrication of high- Q polydimethylsiloxane optical microspheres for thermal sensing", *Applied Physics Letters* 94: 231119 (2009)
- [34] T. Grossmann, S. Schleede, M. Hauser, M. Christiansen, C. Vannahme, C. Eschenbaum, S. Klinkhammer, T. Beck, J. Fuchs, G. Nienhaus, U. Lemmer, A. Kristensen, T. Mapes, and H. Kalt, "Low-threshold conical microcavity dye lasers", *Applied Physics Letters* 96: 013303 (2010)
- [35] F. Gu, F. Xie, X. Lin, S. Linghu, W. Fang, H. Zeng, L. Tong, and S. Zhuang, "Single whispering-gallery mode lasing in polymer bottle microresonators via spatial pump engineering," *Light: science & applications* 6: e17061 (2017)
- [36] Q. Lu, X. Wu, L. Liu, and L. Xu, "Mode-selective lasing in high-Q polymer micro bottle resonators," *Optics Express* 23: 22740-22745 (2015)
- [37] Z. Zhang, N. Yao, J. Pan, L. Zhang, F. Wei, and L. Tong, "A new route for fabricating polymer optical microcavities," *Nanoscale* 11(12), 5203-5208 (2019)
- [38] T. Ioppolo and M. Ötügen, "Magnetochemical polydimethylsiloxane micro-optical resonator," *Opt. Lett.* 35: 2037-2039 (2010)
- [39] A. Alivisatos, K. Johnsson, X. Peng, T. Wilson, C. Loweth, M. Bruchez, P. Schultz, "Organization of 'nanocrystal molecules' using DNA," *Nature* 382, 609-611 (1996)
- [40] I. M. White and X. D. Fan, "On the performance quantification of resonant refractive index sensors," *Opt. Express* 16, 1020-102 (2008)
- [41] R. Kumar, Y. Wang, Y. Zhang, and H. Tsang, "Quantum states of higher-order whispering gallery modes in a silicon micro-disk resonator," *J. Opt. Soc. Am. B* 37, 2231-2237 (2020)
- [42] L. He, S. K. Ozdemir, J. Zhu, and L. Yang, "Scatterer induced mode splitting in poly(dimethylsiloxane) coated microresonators," *Appl. Phys. Lett.* 96(22), 221101 (2010)
- [43] M. Ghulinyan, F. Manzano, N. Prtljaga, M. Bernard, L. Pavese, G. Pucker, and I. Carusotto, "Intermodular reactive coupling induced by waveguide-resonator interaction," *Phys. Rev. A* 90: 053811 (2014)
- [44] J. Zhu, G. Zhao, I. Savukov and L. Yang, "Polymer encapsulated microcavity optomechanical magnetometer," *Sci Rep* 7, 8896 (2017)
- [45] P. Wang, M. Ding, T. Lee, G. S. Murugan, L. Bo, Y. Semenova, Q. Wu, D. Hewak, G. Brambilla, and G. Farrell, "Packaged chalcogenide microsphere resonator with high Q-factor," *Appl. Phys. Lett.* 102, 131110 (2013)